DOI 10.1007/s11003-016-9974-5

Materials Science, Vol.52, No.3, November, 2016 (Ukrainian Original Vol.52, No.3, May–June, 2016)

HYDROGEN RELEASE ON THE ANODE IN THE COURSE OF PLASMA ELECTROLYTIC OXIDATION OF ALUMINUM

L. A. Snezhko,[1,2] A. L. Erokhin,[3] O. A. Kalinichenko,[1] and D. A. Misnyankin[1]

The process of preferential hydrogen release on the anode in the course plasma electrolytic oxidation is a result of the thermochemical reaction between aluminum dispersed in spark discharges and water vapor. It is shown that the products of interaction are aluminum hydroxides or oxides. In this case, the degree of oxidation and the maximum efficiency of the plasma electrolytic oxidation are attained in the case of inhibition of the reaction of hydration of the metal and the presence of sufficient amounts of oxygen in the reaction zone. It is discovered that the compounds present in the electrolyte capable of adsorption on aluminum and the cathodic current component suppress the reaction of aluminum hydration and promote the formation of oxides.

Keywords: electrolytic oxidation, cathodic component, oxide, spark discharge.

Plasma electrolytic oxidation (PEO) is a quite promising procedure of deposition of corrosion- [1], wear- [2], and heat-resistant [3] coatings on aluminum, titanium, and magnesium. As usual, the process is accompanied by the intense release of gases on the anode. Moreover, the composition of these gases and their "anomalous" amount could not be explained [4] within the framework of the available electrochemical regularities. The results of multiple measurements of discharges performed by using different methods [5–8] gave a common knowledge of their parameters (a duration of 0.2–1.0 sec, a temperature of 10^3–10^4°K, and a pressure near the crater of 10^2–10^3 MPa [9]) but did not clarify the nature of thermochemical processes in them. The experimental data obtained earlier [10, 11] reveal large amounts of hydrogen in the anodic gas under the conditions of anodic polarization, which can be explained only by the conversion of aluminum.

In the present work, we study the rate of gas release in the course of plasma electrolytic oxidation of aluminum and analyze the nature of thermochemical processes running in spark discharges.

Experimental Procedure

The process of plasma electrolytic oxidation was studied in an installation depicted in Fig. 1. The role of anode is played by BS 6082 aluminum alloy (0.4–1.0 wt.% Mn; ≤ 0.5 Fe; 0.6–1.2 Mg; 0.7–1.3 Si; ≤ 0.1 Cu; ≤ 0.2 Zn; ≤ 0.1 Ti; ≤ 0.25 Cr; balance Al). The areas of the specimens varied within the range 900–1600 mm^2. The electrolysis was carried out in a solution containing 1 g/liter KOH, 2 g/liter Na_2SiO_3, and 1.5 g/liter $Na_4P_2O_7 \cdot 10\,H_2O$. The temperature of electrolyte was held at 30°C with the help of a water heat exchanger.

[1] Ukrainian State Chemico-Technological University, Dnepropetrovsk, Ukraine.

[2] Corresponding author; e-mail: lsnizhko@mail.ru.

[3] Sheffield University, Sheffield, Great Britain.

Translated from Fizyko-Khimichna Mekhanika Materialiv, Vol.52, No.3, pp.111–119, May–June, 2016. Original article submitted November 19, 2014.

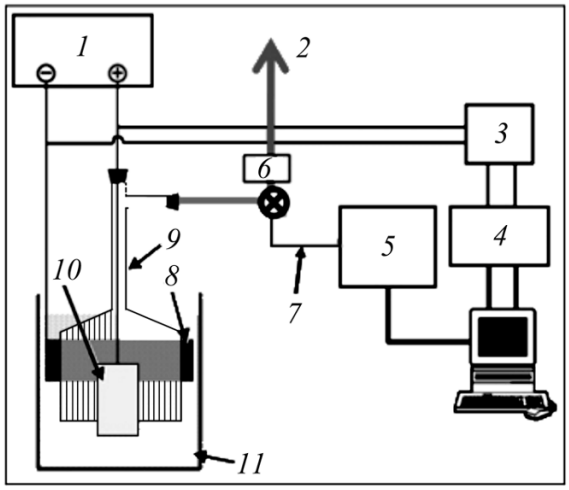

Fig. 1. Experimental installation for PEO with simultaneous collection of the anodic gas: (1) power supply; (2) gas exit; (3) probes for measuring currents and voltages; (4) oscilloscope; (5) gas analyzer; (6) flow gauge; (7) heated capillary; (8) cathode; (9) funnel; (10) anode (working electrode); (11) electrolytic bath.

Table 1. Modes of PEO

No. of the mode	Parameters
1	Direct current $i = 300$ A/m^2
2	Direct current of 600 A/m^2
3	Direct current of 900 A/m^2
4	Unipolar impulsive current $i_{av} = 900$ A/m^2; $f = 100$ Hz
5	Unipolar impulsive current of 900 A/m^2; 1000 Hz
6	Unipolar impulsive current of 900 A/m^2; 10000 Hz
7	Bipolar impulsive current of + 900/– 450 A/m^2; 1000 Hz
8	Bipolar impulsive current of + 900/– 900 A/m^2; 1000 Hz

The procedure of preliminary treatment of the specimens included their mechanical polishing with abrasive paper (to the height of irregularities $R_a \sim 20$ nm) and degreasing with acetone in an ultrasound bath. The specimens were suspended from a threaded joint inside an upturned glass funnel so that the entire gas released from the surface passed through a flow gauge and a gas analyzer. The electrolysis was realized for 600 sec in a galvanostatic mode by applying direct currents in the uni- and bipolar impulsive modes (see Table 1).

The parameters of the process were monitored with the help of a Tektronix TDS 430A oscilloscope equipped with the corresponding probes (A6303-TM502A and P5200A models). The mean values of current and voltage

of the transient processes were recorded with the help of an NI-PXI-5922 digitizer with a frequency of discretization of $1\,\text{sec}^{-1}$.

The density of charge is given by the formula

$$Q = \frac{1}{S}\int i(t)\,dt, \tag{1}$$

where $i(t)$ is the mean current density at time t and S is the area of the specimen surface. The efficiency of the current x_δ (%) spent for the formation of a coating with thickness δ is found as follows:

$$x_\delta = \frac{Q_\delta}{Q}\cdot 100\%, \tag{2}$$

where Q_δ is the amount of electricity (C/m^2) required for the creation of a coating with thickness δ.

To analyze the discharge and composition of the gas, we used a system including a MASS-STREAM (M+W Instruments) flow gauge and a Hiden QGA-200 gas analyzer. The gas was preliminarily dried by passing through a heated capillary. The flow gauge was calibrated by oxygen under the standard conditions (25°C, 101.325 kPa).

If the gas flow contains n components, then the actual release rate of at time t can be determined as follows:

$$v(t) = \frac{v_r(t)}{C_{\text{O}_2}\sum_{i=1}^{n}\dfrac{v_i(t)}{C_i}}, \tag{3}$$

where $C_{\text{O}_2} = 0.98$ is the coefficient of transformation of gaseous oxygen, $v_r(t)$ is the gas flow experimentally measured with the help of the flow gauge, $v_i(t)$ is the volume fraction of gas at time t, and C_i is the factor of conversion of the ith component in the gas mixture.

The quantities $v_i(t)$ can be found according to the results of the gas analysis:

$$v_i(t) = \frac{P_i(t)}{\sum_{i=1}^{n}\left[P_i(t)\right]}. \tag{4}$$

Here, $P_i(t)$ is the partial pressure of the ith component in a gas mixture at the time t of measurements in the gas analyzer.

The total amount of gas mixture V_{mix} formed in the course of plasma electrolytic oxidation can be found as a result of integration of Eq. (3):

$$V_{\text{mix}} = \int v(t)\,dt. \tag{5}$$

Assuming that the gas mixture is collected under the normal pressure, the molar volume of the gas can be found as follows:

$$V_N = \frac{PV_{\text{mix}}}{RT}. \tag{6}$$

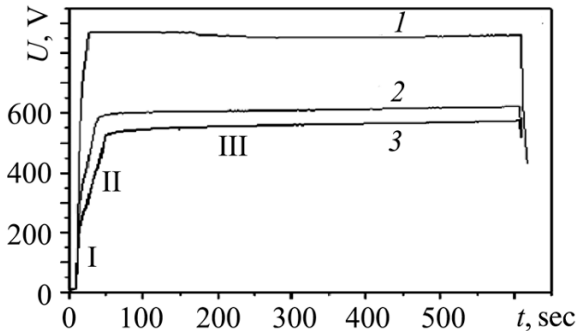

Fig. 2. Voltage-time dependences obtained for a current density of 900 A/m^2 under different conditions of electrolysis: (I–III) stages of the process; (1) mode 7; (2) 5; (3) 3.

Here, P = 101.325 kPa is the normal atmospheric pressure, R = 8.314 J/(K·mole) is the gas constant, and T = 298°K.

The surface of specimens was the studied in a JEOL 6400, 15 kV, scanning electron microscope. The mean porosity of the coatings α was found by analyzing the images of their surfaces with the use of the Image-J software package. The thickness of the coatings was measured in microsections (as the mean value of 15 measurements).

Results and Discussion

It was established (Fig. 2) that the voltage on the electrode increases with different rates. In stage I, it rapidly increases to about 200 V. For the first 13 seconds, the growth rate is as high as ~ 43 V/sec, which is caused, most likely, by the rapid oxidation of aluminum. In stage II with a duration of 13–48 sec, the voltage increases to ~ 500 V at a rate of 8.6 V/sec. In this case, we observe simultaneous appearance of the first gas bubbles and small sparks on the anode. In stage III, the rate decreases to 0.1 V/sec, and the gas release becomes more intense. For the same frequencies, the curves for uni- and bipolar pulses on stage III practically coincide.

The analysis of the surface morphology showed that all coatings made by the plasma electrolytic oxidation have a porous structure. In this case, the size of pores depends on the current density and the electrolysis mode. In modes 1–3 (see Table 1) with an increase in the current density from 300 to 900 A/m^2, their diameter increases by three times, and the mean porosity grows by 8.11%. In modes 4–6, the size of pores decreases, as the frequency of pulses increases. As the frequency of pulses increases from 100 to 10000 Hz, the porosity decreases almost twice. The coatings formed in modes 7 and 8 have a finer porous structure, as compared with the direct current modes and the modes with unipolar pulses. The sizes of pores decrease, as the negative current component increases from – 450 to – 900 A/m^2. In this case, the densest coatings with porosity of 6.84% are obtained in mode 8. We established (see Fig. 3) that the gas mixture consists mainly of hydrogen, nitrogen, oxygen, and atomic particles H and OH. The values of the thickness δ of coatings produced in different modes of the plasma electrolytic oxidation are as follows:

0.95 ± 0.32 μm in mode 1, 2.55 ± 0.83 in mode 2, 3.76 ± 0.73 in mode 3,

4.52 ± 1.22 in mode 4, 4.21 ± 0.85 in mode 5, 3.64 ± 0.59 in mode 6,

2.98 ± 0.79 in mode 7, and 3.57 ± 0.44 μm in mode 8.

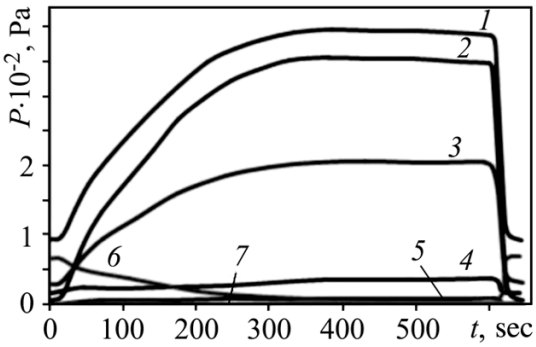

Fig. 3. Partial pressures of the components of anodic gas in the course of PEO for a direct current density of 900 A/m^2: (1) gas mixture; (2) molecular hydrogen (H_2), (3) atomic hydrogen (H); (4) molecular oxygen (O_2); (5) moisture; (6) nitrogen; (7) hydroxyl group (OH).

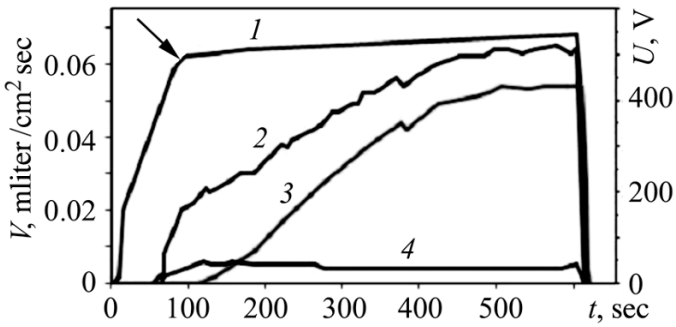

Fig. 4. Voltage–time dependences (1) and the amount of gas released in the course of PEO for a direct current of 600 A/m^2: (2) total gas flow; (3) hydrogen; (4) oxygen.

It is assumed that nitrogen and hydroxyl groups appear in the gas mixture from the admixtures of air and water. Therefore, they are neglected in our subsequent analysis and the gas mixture is normalized to oxygen and hydrogen.

The total amount of molecular hydrogen was calculated with regard for the half amount of atomic hydrogen. To clarify the interconnections between the voltage growth rate and the gas release, the corresponding curves are shown in the same figure (Fig. 4).

The noticeable gas release is observed only if the stable sparking appears at the onset of stage III (at a voltage of about 500 V) approximately after the 48 sec electrolysis (in the direct current mode). For the remaining modes, the time of the onset of a gas collection was determined experimentally. In this case, the composition of a gas was studied only after the pipes of the measuring system were filled. We found that hydrogen becomes the main component of the anodic gas just when the process approaches the mode of stable sparking. In this case, the release of oxygen is suppressed (Fig. 5).

In all modes of electrolysis, the amount of hydrogen is significantly larger than oxygen, which is not consistent with the electrochemical ideas about the nature of the anodic process. As the current density increases from 300 to 900 A/m^2, the specific releases of hydrogen and oxygen increase, respectively, from 1.1 to 49.4 and from 0.08 to 4.6 mliter/cm^2.

The generation of hydrogen is suppressed by the negative current component. Thus, as it varies from 450 to 900 A/m^2 in modes 7 and 8, the hydrogen release decreases from 63.9 to 32.6 mliter/cm^2. The influence of

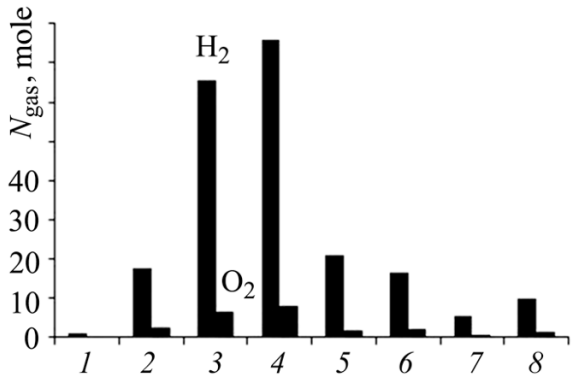

Fig. 5. Experimental correlation between the hydrogen and oxygen contents obtained in the course of PEO for different modes (1–8) of polarization.

the frequency of pulses on the gas release is more complicated. The minimum and maximum amounts of a gas are released at frequencies of 100 and 1000 Hz, respectively. It is obvious that the amount of hydrogen decreases as the frequency of pulses increases (modes 4–6).

The analysis of the rate of gas release allows us to assume that the oxidation in a spark discharge can be considered as a phasic process. First, the primary oxide layer is formed:

$$2\mathrm{Al} + 1.5\mathrm{O_2} \xrightarrow{4\mathrm{OH^-} = 2\mathrm{H_2O} + \mathrm{O_2} + 4e} \mathrm{Al_2O_3}. \tag{7}$$

Then, as spark discharges appear, whose temperature attains several thousand degrees, the chemical elements are atomized:

$$\mathrm{H_2O} \rightarrow 2\mathrm{H} + \mathrm{O}, \quad \Delta E = 910 \text{ kJ/mole}, \tag{8}$$

$$\mathrm{H_2O} + e \rightarrow 2\mathrm{H} + \mathrm{O^-}, \quad \Delta E = 820 \text{ kJ/mole}. \tag{9}$$

It should be taken into account that reactions (8) and (9) are energy consuming to a large extent. For this reason, their fraction in the total energy consumption is at most 10–15% [12].

If the main sources of hydrogen were the water decomposition reactions (8) and (9), its molar content $N_{\mathrm{H_2}}^{\mathrm{H_2O}}$ would be twice larger than oxygen (Fig. 5). Then the amount of such hydrogen could be easily calculated by the experimental content of oxygen in the gas mixture:

$$N_{\mathrm{H_2}}^{\mathrm{H_2O}} = 2N_{\mathrm{O_2}}^{\mathrm{exp}}. \tag{10}$$

Nevertheless, the experimental content of hydrogen in the gas mixture is essentially larger, which supposes the existence of another source generating hydrogen.

It was assumed that the basic reaction supplying hydrogen in the gas mixture is the water-based conversion of aluminum dispersed in spark discharges. The breakdown of oxide causes a local heating of the substrate and the ejection of microparticles of the metal $\mathrm{Al} \rightarrow \mathrm{Al}^*$ into the discharge channel, where the following exother-

mic reactions with water vapor are observed:

$$Al^* + 3H_2O \rightarrow Al(OH)_3 + 1.5H_2, \quad (11)$$

$$Al^* + 2H_2O \rightarrow AlOOH + 1.5H_2, \quad (12)$$

$$Al^* + 1.5H_2O \rightarrow 0.5Al_2O_3 + 1.5H_2. \quad (13)$$

Reactions (11)–(13) are thermodynamically probable in a wide range of temperatures up to the melting of aluminum (660°C). Their thermal effects are, respectively, 16.3, 15.5, and 15.1 MJ/kg Al [13, 14].

The interaction of ejected microparticles of aluminum with water and atomic oxygen results in the formation of various hydroxides in dependence on the stoichiometric ratio between reagents. Unprotected aluminum reacts with water by forming mainly the bayerite forms of hydroxide ($Al(OH)_3$) under a deficit of atomic oxygen and böhmite (AlOOH) or oxide Al_2O_3 under its excess.

It was established in [15, 16] that various products of hydration arise on the anode surface. The amount of atomic oxygen depends essentially on the type and the concentration of an admixture introduced in an electrolyte. The formation of oxygen from water in a spark discharge requires quite high amounts of energy even with participation of electrons. Therefore, due to the deficit of oxygen, the basic products of the electroerosion of aluminum in water are presented by various forms of aluminum hydroxide with domination of its bayerite form. If the concentration of oxygen on the surface is suitable, the Al_2O_3 oxide film hampers the interaction of metallic particles with water [17].

The aluminum oxide in the α-form is formed as a result of the reactions of thermal decomposition of bayerite [18]:

$$\alpha - Al(OH)_3 \xrightarrow{230^\circ C} \eta - Al_2O_3(H_2O) \xrightarrow{850^\circ C} \theta - Al_2O_3(H_2O) \xrightarrow{1200^\circ C} \alpha - Al_2O_3. \quad (14)$$

The substances that contain polymeric silicate- or phosphate-anions form gels of the $SiO_2 \cdot n\,H_2O$ type. These gels are adsorbed on the surface of particles of aluminum and protect them against hydration [19]. The hydrolysis of silicates and the subsequent interaction with aluminum hydroxide can be described by the following reactions:

$$SiO_3^{2-} + 3H_2O \rightarrow H_4SiO_4 + 2OH^-, \quad (15)$$

$$NaOH + Al(OH)_3 + 3H_4SiO_4 \rightarrow NaAlSi_3O_8 + 8H_2O. \quad (16)$$

In view of the compositions of coatings produced by the plasma electrolytic oxidation (α- and β-Al_2O_3) and the ratios of heat effects of reactions (11)–(13), we may assume with high probability that reaction (13) is running in discharges. The mole amount of hydrogen $N_{H_2}^{Al}$, which would be released by this reaction, is determined by the difference between its experimental amount $N_{H_2}^{exp}$ and the amount calculated from the water decomposition reaction:

$$N_{H_2}^{Al} = N_{H_2}^{exp} - N_{H_2}^{H_2O}. \quad (17)$$

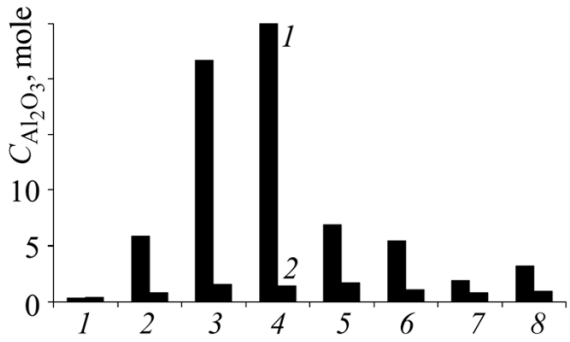

Fig. 6. Correlation between the amounts of Al_2O_3 computed according to the amount of released hydrogen ($N_{Al_2O_3}$) (1) and according to the thickness of the film ($N^{\delta}_{Al_2O_3}$) (2): (1–8) modes of polarization.

Then, according to reaction (13), we compute the molar amount of aluminum oxide $N_{Al_2O_3}$ and aluminum ejected in discharges N_{Al}:

$$N_{Al_2O_3} = \frac{N^{Al}_{H_2}}{3}, \tag{18}$$

$$N_{Al} = N^{Al}_{H_2} * \frac{2}{3}. \tag{19}$$

The experimental amount of oxide ($N^{\delta}_{Al_2O_3}$) is found according to the thickness of the film δ:

$$N^{\delta}_{Al_2O_3} = \frac{\delta S \rho (1-\alpha)}{M_{Al_2O_3}}, \tag{20}$$

where α, ρ, and S are, respectively, the porosity, density of Al_2O_3 (3400 kg/m^3), and the area of the specimen, respectively, and $M_{Al_2O_3}$ is the molar mass of aluminum oxide.

We detected (see Fig. 6) a significant difference between the value given by reaction (13) and the experimental result. In our opinion, this can be explained by the "penetration" of solid products of reactions (11)–(13) into the electrolyte. For a more detailed discussion of the mechanism, it is necessary to study the content of aluminum in the electrolyte.

Since the gaseous products of thermochemical reactions are released through pores, the comparison of their amounts and the efficiencies of growth of the thickness of the coating is of interest to discuss the mechanism of this growth. The efficiency of oxidation is given by the formula (Fig. 7):

$$\eta = \frac{N_{Al_2O_3}}{N^{\delta}_{Al_2O_3}} \cdot 100\%.$$

It is clear that, in modes 1–3, as the current density increases, the efficiency of growth of the thickness of the coating decreases, whereas the level of porosity increases.

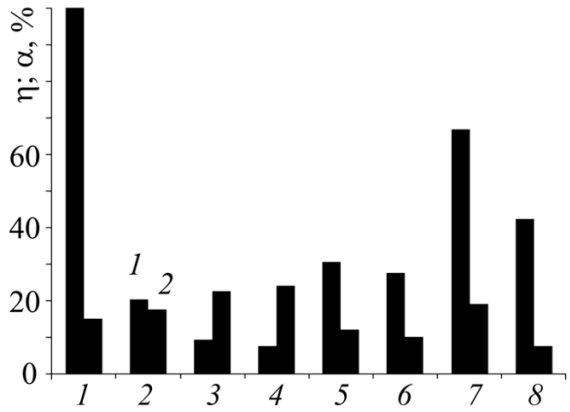

Fig. 7. Efficiency of oxidation (1) and the porosity of coatings (2): (1–8) modes of polarization.

Only for the least current density (300 A/m^2), we observe a correspondence between the computed and actual amounts of oxides (the oxidation efficiency is close to 100%). However, as the current density increases, the indicated balance is violated: the amount of released hydrogen significantly exceeds the amount required for the oxidation of the metal. It is possible to assume that, in this case, the aluminum passes either into a soluble form and forms aluminates in alkaline electrolytes or into the deposits in the form of $Al(OH)_3$ hydroxide.

For a current density of 900 A/m^2 in the DC mode and with unipolar pulses at a low frequency (100 Hz), the porosity of the coatings increases but the positive effect of oxidation decreases.

On the contrary, the efficiency of the process increases with frequency, whereas the porosity of the coatings decreases. In the bipolar mode, we observe a similar effect. Thus, the observed correlation between the efficiency of the process and the porosity of coatings indirectly confirms the fact that the greater the amount of gases released through the channels, the lower the productivity of the process.

The increase in the efficiency of the process under the action of high-frequency pulses is probably caused by the decrease in the duration of action of the current. The duration of spark discharges measured by the optical methods is, on the average, equal to 0.02–0.10 msec [6], which enables us to assume that the optimal conditions are realized on the electrode in the case of coincidence of the duration of a pulse with the time of existence of the discharge. The negative component significantly increases the efficiency of oxidation. The cathodic pulses favor the release of additional amounts of hydrogen as a result of the reduction of water

$$(2H_2O + 2e \rightarrow H_2 + 2OH^-).$$

The thermodynamic regularities imply that the additional amount of hydrogen suppresses both reactions leading to the generation of hydrogen: decomposition of water and conversion of aluminum.

CONCLUSIONS

On the basis on the analysis of the composition of the anodic gas consisting mainly of hydrogen, it is shown that the process of plasma electrolytic oxidation is a combined process. Its first stage is the electrochemical reaction of oxidation of the compact metal (ion transfer); the second stage is the discharge of hydroxyl ions accompanied by the release of gaseous oxygen (electron transfer), and the third stage is the thermochemical conversion of aluminum dispersed in spark discharges. It is discovered that the conversion of aluminum can be accompa-

nied by the formation of hydroxide and oxide forms. Note that the oxide form is preferable because it promotes the formation of the coating. The degree of oxidation of aluminum and the maximum efficiency of the plasma electrolytic oxidation are attained in the presence of sufficient amount of oxygen in the reaction zone. This is attained in the impulsive mode by decreasing the duration of action of discharges and the amount of dispersed aluminum, in the presence of compounds capable of adsorption on aluminum in the electrolyte and its protection against hydration, and by introducing the cathodic current component facilitating hydrogen release and suppressing the conversion of aluminum.

REFERENCES

1. S. Cui, J. Han, Y. Du, and W. Li, "Corrosion resistance and wear resistance of plasma electrolytic oxidation coatings on metal matrix composites," *Surf. Coat. Technol.,* **201**, 5306–5309 (2007).
2. P. A. Dearnley, J. Gummersbach, H. Weiss, A. A. Ogwu, and T. J. Davies, "The sliding wear resistance and frictional characteristics of surface modified aluminium alloys under extreme pressure," *Wear,* **225–229**, 127–134 (1999).
3. J. A. Curran and T. W. Clyne, "The thermal conductivity of plasma electrolytic oxide coatings on aluminium and magnesium," *Surf. Coat. Technol.,* **199**, 177–183 (2005).
4. T. Mizuno, T. Akimoto, and T. Ohmori, "Confirmation of anomalous hydrogen generation by plasma electrolysis," in: *Proceed. of the 4th Meeting of Japan CF Research Society,* Iwate University, Iwate (2003), p. 10.
5. C. S. Dunleavy, I. O. Golosnoy, J. A. Curran, and T. W. Clyne, "Characterisation of discharge events during plasma electrolytic oxidation," *Surf. Coat. Technol.,* **203**, 3410–3419 (2009).
6. C. S. Dunleavy, J. A. Curran, and T. W. Clyne, "Self-similar scaling of discharge events through PEO coatings on aluminium," *Surf. Coat. Technol.,* **211**, 3410–3419 (2011).
7. E. Matykina, A. Berkani, P. Skeldon, and G. E. Thompson, "Real-time imaging of coating growth during plasma electrolytic oxidation of titanium," *Electrochim. Acta,* **53**, 1987–1994 (2007).
8. A. L. Yerokhin, L. O. Snizhko, N. L. Gurevina, A. Leyland, A. Pilkington, and A. Matthews, "Spatial characteristics of discharge phenomena in plasma electrolytic oxidation of aluminium alloy," *Surf. Coat. Technol.,* **177–178**, 779–783 (2004).
9. G. P. Wirtz, S. D. Brown, and W. M. Kriven, "Ceramic coatings by anodic spark deposition," *Mater. Manufact. Proc.,* **6**, 87 (1991).
10. Ye. V. Khokhryakov, P. I. Butyagin, and A. I. Mamaev, "Formation of dispersed particles during plasma oxidation," *J. Mater. Sci.,* **40**, 3007–3008 (2005).
11. S. Moon and Y. Jeong, "Generation mechanism of microdischarges during plasma electrolytic oxidation of Al in aqueous solutions," *Corr. Sci.,* **51**, 1506–1512 (2009).
12. J. Petrovic and G. Thomas, *Reaction of Aluminum with Water to Produce Hydrogen,* U.S. Department of Energy, Washington, DC (2008).
13. A. V. Korshunov, E. B. Golushkova, D. O. Perevezentaeva, and A. P. Il'in, "Macrokinetics of the interaction of electroexplosive nanopowders of aluminum with water and aqueous solutions," *Izv. Tomsk. Politekh. Univ.,* **312**, No. 3, 5–10 (2008).
14. V. V. Zhilinskii, A. K. Lokenbakh, and L. K. Lepin', "Interaction of ultradispered aluminum with water and aqueous solutions," *Izv. Akad. Nauk Latv. SSR. Ser. Khim.,* No. 2, 151–161 (1986).
15. R. K. Bairamov, A. I. Ermakov, and N. R. Vedernikova, "Influence of some organic compounds on the composition of products of the electrospark dispersion of aluminum," *Zh. Prikl. Khim.,* **74**, 1708–1710 (2001).
16. R. K. Bairamov, N. R. Vedernikova, and A. I. Ermakov, "Electrospark dispersion of aluminum and its subsequent hydration," *Zh. Prikl. Khim.,* **74**, 1703–1705 (2001).
17. R. K. Bairamov, "Behavior of metallic particles formed in the course of electrospark dispersion of aluminum in aqueous solutions," *Zh. Prikl. Khim.,* **76**, 1067–1070 (2003).
18. O. V. Al'myasheva, E. N. Korytkova, A. V. Maslov, and V. V. Gusarov, "Preparation of nanocrystalline alumina under hydrothermal conditions," *Neorganich. Mater.,* **41**, No. 5, 460–467 (2005); ***English translation****: Inorganic Mater.,* **41**, No. 5, 460–467 (2005).
19. J. R. Morlidge, P. Skeldon, G. E. Thompson, H. Habazaki, K. Shimizu, and G. C. Wood, "Gel formation and the efficiency of anodic film growth on aluminium," *Electrochim. Acta,* **44**, 2423–2435 (1999).